arXiv:1602.04371v1 [cond-mat.mes-hall] 13 Feb 2016

Superconducting-contact-induced resistance-anomalies in the 3D topological insulator Bi_2Te_3

Zhuo Wang,[1] Tianyu Ye,[1] and R. G. Mani[1]

[1]*Department of Physics and Astronomy, Georgia State University, Atlanta, GA 30303.*

(Dated: February 16, 2016)

Abstract

This study examines the magnetotransport response observed in flakes of the 3D topological insulator Bi_2Te_3, including indium superconducting electrodes, and demonstrates two critical transitions in the magnetoresistive response with decreasing temperatures below $T = 3.4$ K. The first transition is attributed to superconductivity in the indium electrodes, and the second transition, with a critical field exceeding the transition field of indium, is attributed to a proximity effect at the 2D planar interface of this hybrid TI/superconductor structure.

Topological insulators (TI) are 2- and 3-dimensional electronic materials that behave as a normal insulator in the bulk but conduct electricity in edge or surface states, respectively, that arise from a bulk-boundary correspondence, and are topologically protected by time-reversal symmetry.[1–3] TI are characterized by a strong spin-orbit coupling that provides a locking between spin and linear momentum, and the helical spin polarization as gapless surface states exhibit a linear dispersion relation, i.e., "Dirac cones," characteristic of relativistic massless particles. The $CdTe/HgTe/CdTe$ quantum well system was the first theoretically predicted[4] and experimentally demonstrated[5] 2D TI, followed by the prediction[8] and experimental confirmation[9] of the technological significant $AlSb/InAs/GaSb/AlSb$ quantum well system as another 2D TI. $Bi_{1-x}Sb_x$ was the first theoretically predicted- and experimentally identified-3D TI.[6, 7] Since then, a large number of other systems with a band-gap $E_0 \leq 0.3\ eV$ at 300 K including Bi_2Se_3,[10] Sb_2Te_3,[11] and Bi_2Te_3,[12, 13] have joined the class of 3D TI. Remarkably, among these systems, Bi_2Se_3 has exhibited superconductivity with a critical transition temperature of $T_c = 3.8$ K, when copper is intercalated between the adjacent quintuple layers.[14, 15] Further, the application of pressure in the range of 3-6 GPa in Bi_2Te_3 has been shown to induce superconductivity with $T_c \approx 3$ K and $B_c(1.8\text{ K}) \approx 0.2$ T.[16]

The proximity effect from an ordinary s-wave superconductor in the TI leads to exotic $p_x + ip_y$ superconductivity capable of hosting Majorana fermions, and this prediction has heightened interest in experimental studies of superconductor-topological insulator hybrid devices.[17, 18] Thus, many have examined TI nanowire-superconductor devices in search of Majorana modes at the ends of one dimensional devices.[19–24] Nevertheless, a two-dimensional experimental setting for the study of Majorana modes is desirable. In Ref. [17], superconductivity is induced in the surface state of the TI by the proximity effect produced by an ordinary s-wave superconductor, and the Majorana mode is a vortex bound state at the interface of the two materials. Recently, there has been interest in whether—in systems now called "topological metals," which include 3D TI materials such as Bi_2Te_3 and Bi_2Se_3 that have bulk states coexisting with surface states at the Fermi energy—it is possible for the proximity effect to extend from the superconductor covered surfaces to uncovered surfaces of the 3D TI[25] and whether the uncovered surfaces of the 3D TI can thus host Majorana modes.[26] In moving towards exploring such possibilities, we have examined the magnetotransport response in the 3D topological insulator Bi_2Te_3 in the presence of

(indium) topside superconducting electrodes.[27–32] Remarkably, the experimental results showed two critical transitions in the magnetoresistive response below $T = 4.2$ K. While the first transition is associated with a shunting effect by the contacts, the second anomalous contribution, which indicates $T_c \approx 3.1$ K and $B_c(1.5\text{ K}) \approx 0.2$ T, is attributed here to a generalized proximity effect in the TI.

Bi_2Te_3 flakes ($\approx 25\mu m$ thick) were mechanically exfoliated using a scotch tape method from single crystals of Bi_2Te_3 and transferred onto Si/SiO_2 substrates. The Bi_2Te_3 flakes were approximately shaped like rectangles with the length-to-width ratio $L/W \approx 2$. Superconductor/topological insulator junctions were realized by directly pressing indium onto the surface of the Bi_2Te_3 flake in a Hall bar configuration; see supplementary material for the images of the samples.[33] Here, indium is a s-wave superconductor with the critical temperature $T_c = 3.41$ K.[34] Electrical measurements were carried out using the standard four-terminal low-frequency lock-in techniques, and all the reported resistances are four-terminal resistances. The *ac* was applied along the long axis of the Hall bar, through electrodes at the two ends, and the magnetic field was applied perpendicular to the Hall bar surface, as usual. Since the flakes are not so thin, the applied current is carried by both the specimen bulk and the specimen surfaces. Further, since the proximity effect should be restricted to the near surface regions, one expects to observe just resistance corrections due to the proximity effect in the measured four terminal resistances. That is, one does not expect the four terminal resistance to vanish even with the onset of superrconductivity in the contacts and the proximity effect in the surfaces near the contacts. The specimens were immersed in pumped liquid Helium, and the temperature was varied in the range $1.6 \leq T \leq 4.2$ K by controlling the vapor pressure of liquid helium within a ^{4}He cryostat. Hall effect measurements indicated the carrier concentration $n \approx 10^{19} cm^{-3}$ in these samples.

Fig. 1a shows a color plot of the normalized magnetoresistance, $\Delta R/R$ as a function of both the magnetic field, B, and the temperature, T, for sample 1. Here, $\Delta R/R = [R(B) - R(B_N)]/R(B_N)$, where $B_N = -0.3$ T. The color plot (Fig. 1(a)) shows a set of horizontal and vertical lines, which correspond to constant B- and T-cross-sections, which are exhibited in Fig. 1(b) and Fig. 1(c), respectively. In the $T = 3.6$ K cross-section, shown in light green (see Fig. 1(b)), sample 1 shows a featureless $\Delta R/R$, with a small positive magnetoresistance of 0.3 T.[33] However, at 3.4 K, which is slightly below the superconducting transition temperature of indium, $\Delta R/R$ exhibits a sharp and narrow dip near zero magnetic field. As

the temperature is reduced further, this dip in $\Delta R/R$ rapidly becomes deeper until $T = 3.1$ K, as its width along the B-axis, denoted here as ΔB_1, increases. A close examination of $\Delta R/R$ suggests the emergence of a second $\Delta R/R$ contribution for $T \leq 3.0$ K in this specimen. The width but not the depth of this second contribution to $\Delta R/R$ grows rapidly with decreasing T. At $T = 1.7$ K, the critical magnetic field is denoted as $B_{c2}(1.7\text{ K}) = \Delta B_2/2 \approx 0.18$ T. Fig.1(c) depicts the magnitude of $\Delta R/R$ vs. T at the constant-B cross-sections shown in Fig. 1(a) . This figure shows that, with decreasing temperatures, the $\Delta R/R$ drops within a small ΔT interval and then plateaus. The ΔT interval where the drop is observed depends upon B. The temperature dependence of the critical fields associated with the two contributions, i.e., B_{c1} and B_{c2}, are shown in Fig.1 (d). Here, the critical fields were determined by examining the first derivative of the magnetoresistance data and identifying the magnetic fields where the slope, dR_{xx}/dB, exhibits a substantial change. The results of Fig. 1(d) indicate an approximately linear relationship between the critical fields and temperature for the two contributions to $\Delta R/R$.

The results for a second Bi_2Te_3 specimen are shown in Fig. 2. The top panel in Fig. 2 shows a color plot of $\Delta R/R$ vs. B and T, with five horizontal- and three vertical-cross sections. The data corresponding to the horizontal-cross sections are shown in Fig. 2(b). Here, $\Delta R/R$ shows an initial negative magnetoresistance followed by a weak positive magnetoresistance at 3.6 K(see Fig.2(b)). Fig. 2 (b) also shows a rapid dip in $\Delta R/R$ beginning at $T = 3.4$ K in the vicinity of $B = 0$. A second resistance correction term is readily apparent by 2.8 K, and this term mainly gains width but not depth with the decreasing temperature. At $T = 2.0$ K, the critical magnetic field is denoted as $B_{c2}(2.0\text{ K}) = \Delta B_2/2 \approx 0.12$ T in this specimen. The temperature dependences of the critical fields associated with the two contribution, i.e., B_{c1} and B_{c2}, are shown in Fig. 2(d). The results indicate an approximately linear increase in the critical fields with the decreasing temperatures. The vertical (constant magnetic field) cross sections indicated in Fig. 2(a) are shown in Fig. 2(c). As in Fig. 1(c), Fig.2(c) shows that, with decreasing temperatures, the $\Delta R/R$ drops within a small ΔT interval and then plateaus. The T-band where the drop is observed depends again upon B.

A color plot of normalized magnetoresistance for a third Bi_2Te_3 specimen, sample 3, is shown in Fig. 3(a). The data corresponding to the horizontal-cross sections are shown in Fig. 3(b). Here, $\Delta R/R$ shows predominantly negative magnetoresistance at the highest

temperatures. Fig. 3 (b) also shows a small sharp dip in $\Delta R/R$ in the $T = 3.3$ K data trace in the vicinity of $B = 0$. The dip quickly reaches its maximum depth near $T = 2.9$ K. With a further reduction in T, the resistance correction rapidly increases in width. The constant magnetic field cross sections indicated in Fig. 3(a) are shown in Fig. 3(c). As for specimens 1 and 2, the $\Delta R/R$ drops within a small ΔT interval and then plateaus.

This magnetotransport study of Bi_2Te_3 with indium contacts shows the following features: (a) Above the superconducting transition temperature of indium, the specimens show either a weak positive (Fig. 1 (b)), mixed type (Fig. 2(b)), or weak negative (Fig. 3(b)) magnetoresistance. This aspect will be examined in greater detail elsewhere. At the moment, we attribute the observed differences in the normal state magnetoresistance characteristics to variations in the concentration of tellurium vacancies in the bulk crystals utilized to realize these specimens. (b) Below the transition temperature of indium, $T_c = 3.41$ K,[34], there is a sharp drop in the resistance in the vicinity of $B = 0$, which grows rapidly with decreasing temperatures down to $T \approx 2.9$ K. The critical magnetic field associated with this resistance correction is $B_{c1} = \Delta B_1/2 < B_c^{In}(0\text{ K})$, consistent with the known critical field for indium, $B_c^{In}(0\text{ K}) = 0.0281$ T.[35] (c). Below $T \approx 3.1$ K, there appears an additional correction in $\Delta R/R$ which mainly affects the width of the resistance anomaly with the decreasing temperatures. The critical magnetic field associated with this term $B_{c2} = \Delta B_2/2 \leq 0.2$ T easily exceeds the critical field of indium. (d) Constant magnetic field cross sections show that the drop in the resistance occurs over a narrow temperature range (see Fig. 1(c), 2(c), and 3(c)), and this is followed by an apparent plateau in the temperature dependence of $\Delta R/R$. Due to the correlation of the observed effects with superconductivity in the contacts, one may, at the outset, rule out weak localization and electron-interactions as the origin of the observed magnetoresistance anomalies.[36–39]

When a normal metal (N) is brought into good contact with a superconductor (S), Cooper pairs from the superconductor can leak into the normal metal and help to manifest signs of superconductivity in N, while weakening the superconductivity in S.[40] The spatial extent of the proximity effect in N depends also on the presence of impurities and disorder dependent dephasing mechanisms in N.[41] Thus, Andreev reflection theory encompasses both the ideal ballistic N-S interfaces, as well as real-world N-S systems in the diffusive limit (see, for example, Ref.[42]).

One possible image for the observed effects is presented in Fig. 4. The voltage and current

probes (see Fig. 4(a)) used in these experiments consist of the s-wave superconductor indium. Fig. 4(b) illustrates the four terminal transport measurement at $T > T_{c1}$. In this high temperature condition, the voltage probes behave as normal metals. Further, the applied current is transported by the surface states of the TI as well as by the bulk of Bi_2Te_3. When the temperature is reduced to $T < T_{c1}$, the current and voltage probes become superconducting (see Fig. 4(c)), and some additional current next to the surface is shunted through the contacts with the onset of superconductivity in indium, and the contact shunt current path is favored over the current path within the TI. This effect explains the resistance drop associated with ΔB_1 in the $\Delta R/R$ data. A further decrease in the temperature could result in a leakage of Cooper pairs into the topological insulator (see Fig. 4(d)), which can be characterized by a critical temperature $T_{c2} \leq T_{c1}$. If this proximity superconductivity layer shunts additional current, there will be another correction in the resistance, and this could provide for the observed broad resistance correction at the lowest temperatures in our specimens.

There is, however, the observable feature that the critical field $B_{c2} = \Delta B_2/2$ is as large as 0.2 T at the lowest temperatures. This B_{c2} exceeds by nearly a factor-of-ten the critical field of indium, $B_c^{In}(0\text{ K})$. From our understanding, it is not possible to have a proximity effect in the neighboring normal metal above the critical field of the superconductor.

Note, however, the reported result that Bi_2Te_3 exhibits superconductivity under the application of pressure in the range of 3–6 GPa.[1] Further, Ref.[16] indicates that induced superconductivity in Bi_2Te_3 tends to exhibit a $T_c \approx 3$ K and $B_c \approx 0.2$ T.[16] Remarkably, our data also indicate a $T_{c2} \approx 3.1$ K and $B_{c2} \leq 0.2$ T. This point suggests that the second critical transition associated with B_{c2} could originate from a contact induced surface modification in the Bi_2Te_3 flake, which mimics the effect of pressure, but only in the immediate area under the contact.

[1] M. Z. Hasan, and C. L Kane, Rev. Mod. Phys. 82, 3045 (2010).

[2] X. L. Qi, and S. C. Zhang, Rev. Mod. Phys. 83, 1057 (2011).

[3] Y. Ando, J. Phys. Soc. Jpn. 82, 102001 (2013).

[4] B. A. Bernevig, T. l. Hughes, and S. C. Zhang, Science 314 1757 (2006).

[5] M. Konig, S. Weidmann, C. Brune, A. Roth, and H. Buhmann, Science 318, 766 (2007).

[6] L. Fu, and C. L. Kane, Phys. Rev. B 76, 045302 (2007) .

[7] D. Hsieh, D. Qian, L. Wray, Y. Xia, Y. S. Hor, R. J. Cava, and M. Z Hasan, Nature 452, 970 (2008).

[8] C. Liu, T. L. Hughes, X. L. Qi, K. Wang, and S. C. Zhang, Phys. Rev. Lett. 100, 236601 (2008).

[9] I. Knez, R. R. Du, and G. Sullivan, Phys. Rev. Lett. 107, 136603 (2011).

[10] Y. Xia, D. Qian, D. Hsieh, L. Wray, A. Pal, H. Lin, A. Bansil, D. Grauer, Y. S. Hor, R. J. Cava, and M. Z. Hasan, Nat. Phys. 5, 398 (2009) .

[11] Y. Jiang, Y. Wang, M. Chen, Z. Li, C. Song, K. He, L. Wang, X. Chen, X. Ma, and Q-K. Xue, Phys. Rev. Lett. 108 016401 (2012) .

[12] Y. L. Chen, J. G. Analytis, J-H. Chu, Z. K. Liu, S. K. Mo, X. L. Qi, H. J. Zhang, D. H. Lu, X. Dai, Z. Fang et al., Science 325, 178 (2009).

[13] D. Hsieh, Y. Xia, D. Qian, L. Wray, F. Meier, J. H. Dil, J. Osterwalder, L. Patthey, A. V. Fedorov, H. Lin, et al., Phys. Rev. Lett. 103 146401 (2009).

[14] Y. S. Hor, A. J. Williams, J. G. Checkelsky, P. Roushan, J. Seo, Q. Xu, H. W. Zandbergen, A. Yazdani, N. P. Ong, and R. J. Cava, Phys. Rev. Lett. 104, 057001 (2010).

[15] S. Sasaki, M. Kriener, K. Segawa, K. Yada, Y. Tanaka, M. Sato, and Y. Ando, Phys. Rev. Lett. 107, 217001 (2011).

[16] J. L Zhang, S. J. Zhang, H. M. Weng, W. Zhang, L. X. Yang, Q. Q. Liu, S. M. Feng, X.C. Wang, R. C. Yu, L. Z. Cao et al., Proc. natl. Acad. Sci. U.S.A. 108, 24-28 (2011).

[17] L. Fu, and C. L. Kane, Phys. Rev. Lett. 100, 096407 (2008).

[18] C. Nayak, S. H. Simon, A. Stern, M. Freedman, and S. Das Sarma, Rev. Mod. Phys. 80, 1083 - 1159 (2008).

[19] V. Mourik, K. Zuo, S. M. Frolov, S. R. Plissard, E. P. A. M. Bakkers, and L. P. Kouwenhoven,

Science 336, 1003 (2012).

[20] A. Das, Y. Ronen, Y. Most, Y. Oreg, M. Heiblum, and H. Shtrikman, Nat. Phys. 8, 887 (2012).

[21] L. P. Rokhinson, X. Liu, and J. K. Furdyna, Nat. Phys. 8, 795 (2012).

[22] M. T. Deng, C. L. Yu, G. Y. Huang, M. Larsson, P. Caroff, and H. Q. Xu, Nano Lett. 12, 6414 (2012).

[23] W. Chang, V. E. Manucharyan, T. S. Jespersen, J. Nygard, and C. M. Marcus, Phys. Rev. Lett. 110, 217005 (2013).

[24] A. D. K. Finck, D. J. Van Harlingen, P. K. Mohseni, K. Jung, and X. Li, Phys. Rev. Lett. 110, 126406 (2013).

[25] M. X. Wang, H. Ding, A. V. Fwdorov, W. Yao, Z. Li, Y. F. Lv, K. Zhao, L. G. Zhang, Z. Xu, J. Schneeloch et al., Science 336, 52 - 55 (2011).

[26] K. Lee, A. Vaezi, M. H. Fischer, & E. A. Kim, Phys. Rev. B 90, 214510 (2014).

[27] R. G. Mani, L. Ghenim, and T. Theis, Phys. Rev. B 45, 9877 (1992).

[28] L. Ghenim, and R. G. Mani, Appl. Phys. Lett. 60, 2391 (1993).

[29] D. Zhang, J. Wang, A. M. DaSilva, J. S. Lee, H. R. Gutierrez, Moses H. W. Chan, J. Jain, and N. Samarth, Phys. Rev. B 84, 165120 (2011).

[30] F. Yang, Y. Ding, F. Qu, J. Shen, J. Chen, Z. Wei, Z. Ji, G. Liu, J. Fan, C. Yang et al., Phys. Rev. B 85, 104508 (2012).

[31] M. Veldhorst, M. Snelder, M. Hoek, T. Gang, V. K. Guduru, X. L. Wang, U. Zeitler, W. G. Van der Wiel, A. A. Golubov, H. Hilgenkamp, and A. Brinkman, Nature Mater. 11, 417 (2012).

[32] F. Qu, F. Yang, J. Shen, J. Chen, Z. Ji, G. Liu, J. Fan, X. Jing, C. Yang, and L. Lu, Scientific Reports 2, 339 (2012).

[33] See supplementary material at http://dx.doi.org/10.1063/1.4934871 for sample-pictures and magnetotransport data examining the normal states.

[34] See http://www.superconductors.org/type1.htm for Type 1 superconductor properties and a periodic chart comparison (2007).

[35] M. Tinkham, *Introduction to Superconductivity*. 2nd edn (McGraw Hall, New York, 1996).

[36] G. Bergmann, Phys. Rep. 107, 1 (1984).

[37] M. Liu, J. Zhang, C. Chang, Z. Zhang, X. Feng, K. Li, K. He, L. Wang, X. Chen, X. Dai, et

al., Phys. Rev. Lett. 108, 036805 (2012).

[38] R. G. Mani, A. Kriisa, and W. Wegscheider, Sci. Rep. 3, 2747 (2013).

[39] R. G. Mani, L. Ghenim, and J. B Choi, Phys. Rev. B43, 12630 (1991).

[40] G. Blonder, M. Tinkham, and T. M. Klapwijk, Phys. Rev. B 25, 4515 (1982).

[41] T. M. Klapwijk, J. Supercond: Incorp. Novel Magnetism, 17, 593 (2004).

[42] S. Gueron, H. Pothier, N. O. Birge, D. Esteve, and M. H. Devoret, Phys. Rev. Lett. 77, 3025 - 3028 (1996).

ACKNOWLEDGEMENTS

Z.W., T.Y., and magnetotransport studies in Georgia State University have been supported by the U.S. Department of Energy, Office of Basic Energy Sciences, Material Sciences and Engineering Division under DE-SC0001762. Additional support has been provided by the ARO under W911NF-14-2-0076.

AUTHOR CONTRIBUTIONS

Measurements were done by Z.W. Technical assistance was given by T.Y. Experimental development and manuscript was written by Z.W. and R.G.M. The authors declare no competing financial interests.

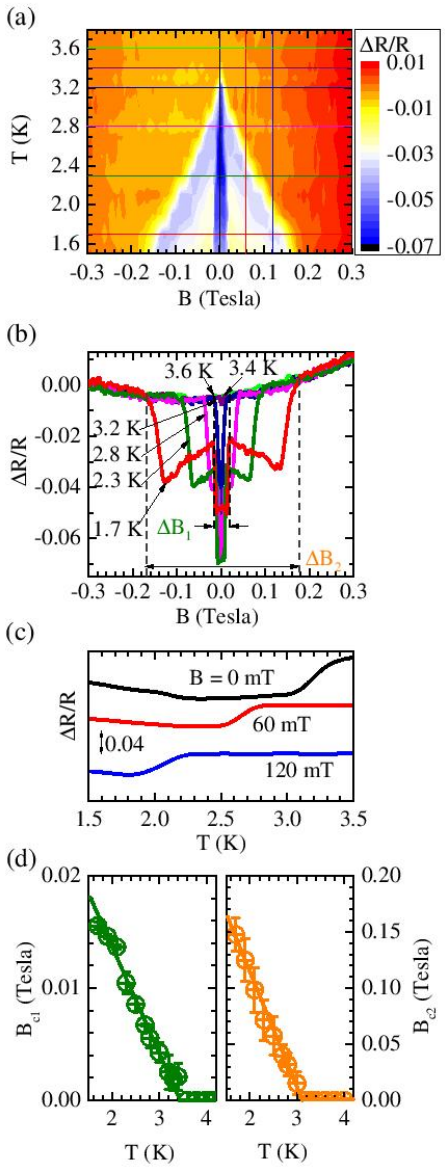

FIG. 1. **Transport in Bi_2Te_3 flakes including indium contacts.** (a) A 2D color plot of the normalized magnetoresistance, $\Delta R/R$, is shown vs. the magnetic field, B, and the temperature, T, for a Bi_2Te_3 specimen, sample 1. (b) This panel exhibits the normalized magnetoresistance vs. B, at the T-cross-sections indicated in panel (a). (c) This panel shows the temperature-dependence of $\Delta R/R$ at zero magnetic field. (d) The critical fields B_{c1} and B_{c2} are plotted on the left and right, respectively, vs. T. Data are shown as symbols. Lines represent the trend.

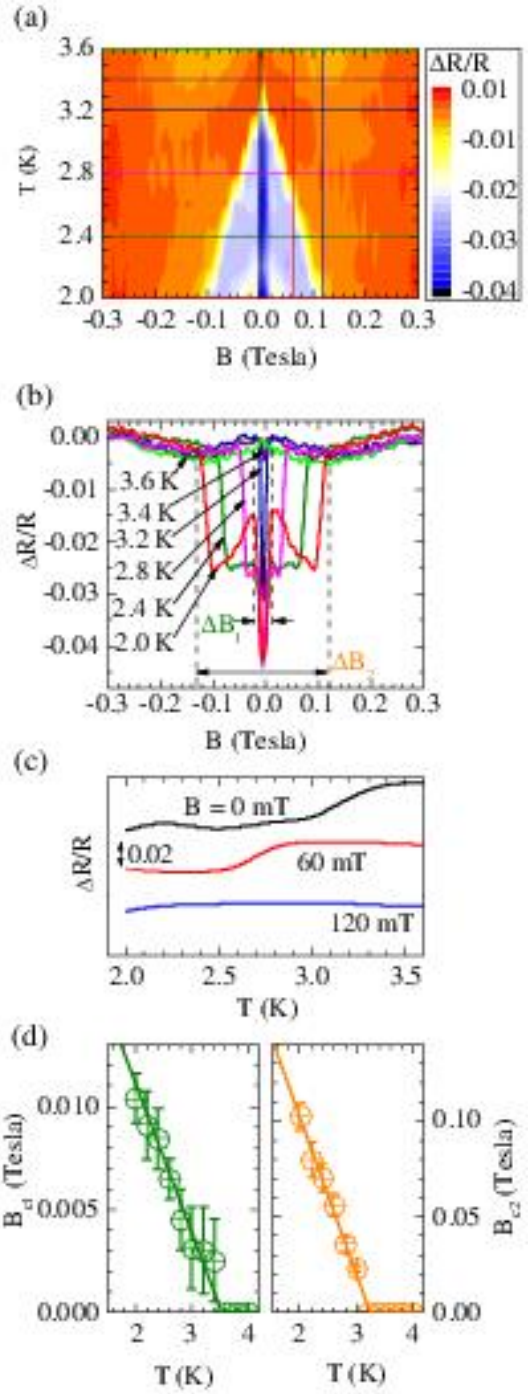

FIG. 2. **Transport in Bi_2Te_3 flakes including indium contacts.** (a) A 2D color plot of the normalized magnetoresistance, $\Delta R/R$, is shown vs. the magnetic field, B, and the temperature, T, for a Bi_2Te_3 specimen, sample 2. (b) This graph exhibits the normalized magnetoresistance vs. B, at the T-cross-sections indicated in the top panel. (c) This panel compares the temperature dependence of the normalized resistance at $B =$ 0 mT, $B =$ 60 mT, and $B =$ 120 mT. (d) The critical fields B_{c1} and B_{c2} are plotted on the left and right, respectively, vs T Data are shown as symbols. Lines represent the trend.

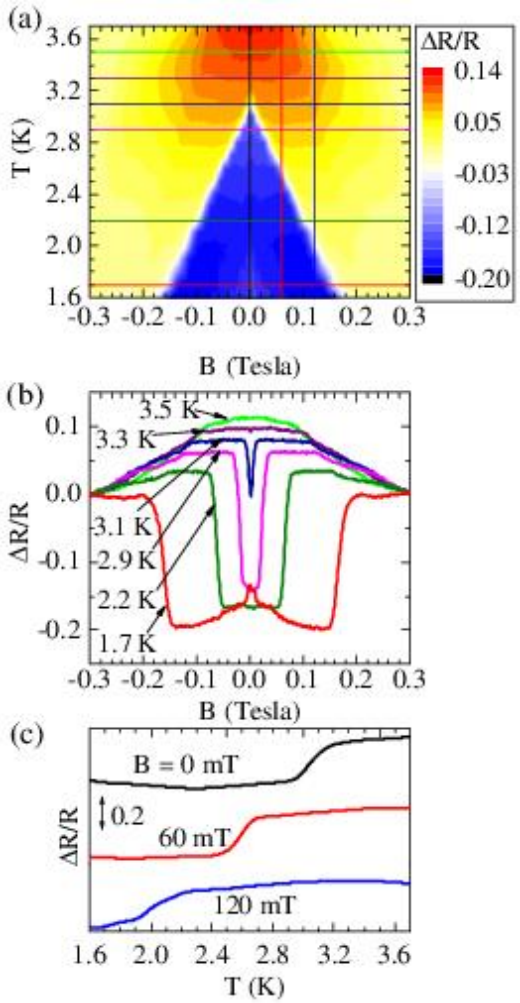

FIG. 3. **Transport in Bi_2Te_3 flakes including indium contacts.** (a) This figure shows a 2D color plot of normalized magnetoresistance, $\Delta R/R$, vs. the magnetic field, B, and the temperature, T, for a Bi_2Te_3 specimen, sample 3. (b) The normalized magnetoresistance, $\Delta R/R$, vs. B, is shown at the different T cross-sections indicated in the top panel. (c) This panel compares the T-dependence of the normalized resistance at the magnetic field cross-sections at $B = 0$ mT, $B = 60$ mT, and $B = 120$ mT.

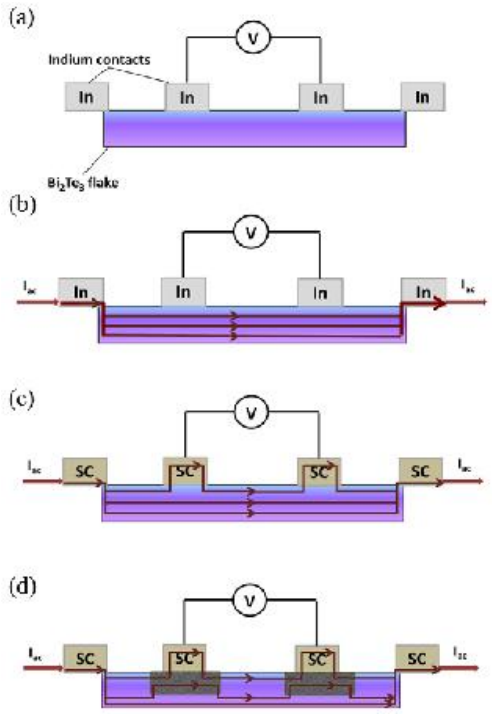

FIG. 4. **Possible scenario for observed effects.** A traditional proximity effect based explanation for the observed effects: (a) A sketch of a Bi_2Te_3 flake with superconducting indium contacts. (b) A Bi_2Te_3 flake with a bulk current in the normal state above the contact superconducting transition critical temperature, T_{c1}. (c) Below the T_{c1}, some additional fraction of the current I is shunted through the contacts when the contacts are in the superconducting state. (d) Below the critical temperature, T_{c2}, associated with the proximity effect, Cooper pairs on the TI side of the interface provide an additional shunt for the current.